electronics

Article

Research on a Torque Ripple Suppression Method of Fuzzy Active Disturbance Rejection Control for a Permanent Magnet Synchronous Motor

Congxin Lv [1,*], Bo Wang [2], Jingbo Chen [2], Ruiping Zhang [1], Haiying Dong [3,*] and Shaoqi Wan [3]

[1] College of Automation and Electrical Engineering, Lanzhou Jiaotong University, Lanzhou 730070, China; zhrp74@mail.lzjtu.cn
[2] Academy, Lanzhou Wanli Airlines Electromechanical Limited Liability Company, Lanzhou 730070, China; wangb18306782.135@mail.avic (B.W.); chenjb18708803.135@mail.avic (J.C.)
[3] College of New Energy and Power Engineering, Lanzhou Jiaotong University, Lanzhou 730070, China; 12212033@stu.lzjtu.edu.cn
* Correspondence: 11210380@stu.lzjtu.edu.cn (C.L.); hydong@mail.lzjtu.cn (H.D.)

Abstract: In order to meet the necessities of steady and protected operation of a permanent magnet synchronous motor (PMSM) in electromechanical pressure gadget aviation beneath complicated working conditions, a three-phase four-arm inverter fuzzy self-disturbance suppression management (Fuzzy-ADRC) approach for PMSM is proposed to suppress the motor torque pulsation beneath complicated working conditions. Firstly, the defects of the common inverter are analyzed, the three-phase four-bridge inverter is changed via the standard three-phase three-bridge inverter, and the present-day harmonic suppression's overall performance of the three-phase four-bridge inverter is modeled, analyzed, and verified. Secondly, the ADRC and fuzzy management approach is analyzed, the Kalman filter is delivered into the motor pace loop management to enhance the overall performance of ADRC, and then the fuzzy manipulate and ADRC are blended to similarly enhance the torque ripple suppression's overall performance of the everlasting magnet synchronous motor. Finally, the proposed three-phase four-arm inverter and fuzzy-ADRC approach are combined, and contrasted with the normal three-phase three-arm inverter and ADRC method. The simulation consequences exhibit that the proposed manipulation technique can efficiently suppress the torque ripple of everlasting magnet synchronous motor and has robust reliability.

Keywords: PMSM; three-phase four-leg inverter; load sudden change; ADRC; fuzzy control; torque ripple

check for updates

Citation: Lv, C.; Wang, B.; Chen, J.; Zhang, R.; Dong, H.; Wan, S. Research on a Torque Ripple Suppression Method of Fuzzy Active Disturbance Rejection Control for a Permanent Magnet Synchronous Motor. *Electronics* **2024**, *13*, 1280. https://doi.org/10.3390/electronics13071280

Academic Editor: Kan Akatsu

Received: 20 February 2024
Revised: 16 March 2024
Accepted: 27 March 2024
Published: 29 March 2024

1. Introduction

PMSM is widely used in various motor driving applications because of its simple structure, stable speed, high reliability, and high efficiency [1–3]. The development of rare earth materials and modern power electronic control technology has further improved the control performance of PMSM, so the aviation electromechanical actuator system also uses a large number of PMSMs with superior performance [4,5].

PID control is extensively used in motor manipulation structures in a range of fields due to its ease and handy parameter adjustment. However, aviation electromechanical actuation systems often have to face extremely harsh working environments, such as low-temperature turbulence, and the external disturbance changes greatly, which requires very high disturbance resistance and robustness of the control system. However, simple PID control can only be applied to areas with low motor stability and safety requirements, and it is convenient to produce giant overharmonic torque ripple in the face of load conditions such as the unexpected alternate of the motor load. The predictive flux control model proposed by Gao et al. [6] introduced the zero vector into the alternative vector set to reduce the current harmonic content and quickly selects the voltage vector according to the flux error vector, which reduces the torque ripple of the motor. Wang et al. [7] proposed a new kind of lengthy predictive time area direct modern mannequin predictive management method, which effectively reduces the current harmonics and torque ripple of the motor. MohammadHadi et al. [8] proposed that non-stop manipulation set mannequin predictive management has the capacity to tune reference values with zero steady-state error for motor controllers. This technique can also achieve a quick dynamic response to motors, with a complete harmonic distortion that is significantly lower than that of finite manage set mannequin predictive control. Chen et al. [9] analyzed the impact of a number of parameters on the motor torque in accordance with the distinct influencing elements via the finite thing model and proposed that the no-load torque of the motor should be suppressed by way of optimizing the structural parameters of the motor, and the ripple torque of the motor should be suppressed by optimizing the winding position.

Zhou et al. [10] combined as genetic algorithm and TOPSIS method to optimize the global multi-objective motor and improve the torque ripple suppression ability of the high-speed motor. At the same time, the method of suppressing motor torque pulsation based on harmonic current injection [11,12] studied by a large number of scholars has become more mature. Wang et al. [13] proposed an adaptive linear neural network harmonic injection method based on biased current input. Based on the cross-coupling effect of the motor, Zheng et al. [14] proposed an approach of motor torque ripple inhibition primarily based on optimum harmonic present-day injection. Wu et al. [15] proposed a highest-quality-voltage harmonic injection speed harmonic minimization approach based totally on amplitude and section evaluation of the influence of injection voltage harmonic amplitude and section on speed harmonic amplitude. Guo et al. [16] proposed a torque ripple suppression approach considering the harmonic flux segment angle, built a goal feature considering each torque ripple and loss minimization with the aid of deducing a torque mannequin considering harmonic flux, and optimized the best harmonic modern by means of a genetic algorithm. Hyung-Jin et al. [17] utilized adaptive manipulation to compensate for the torque ripple of the motor. Zhang et al. [18] blended the three-parameter notch filter and linear lively disturbance rejection controller to suppress the contemporary harmonics of the motor, which weakens the impact of the present-day harmonics on the torque's overall performance of the motor. Based on the evaluation of the relationship between the pulsation aspect in the torque and the modern-day pulsation factor in the motor, Zhou et al. [19] proposed an improved closed-loop frequency compensation strategy to eliminate the pulsation component in the motor torque. Huang et al. [20] introduced fractional order operation into the resonant controller and designed a robust internal model controller.

In addition, many scholars whose studies were based totally on PI management and energetic disturbance rejection manipulation studied motor torque ripple suppression strategies. Yuan et al. [21] proposed a current double closed-loop control strategy with PI control in the inner loop and repeated control in the outer loop. Wang et al. [22] suppressed the modern torque of the motor by way of designing a Chebyshev filter blended with PI control. Based on the evaluation of singular perturbation idea and common theorem, Tian et al. [23] proposed a current loop adaptive disturbance rejection control. Liu et al. [24] accelerated the lively disturbance rejection management via the usage of the prolonged country observer in a parallel resonant unit, which can efficiently suppress the torque pulsation of zero sequence current and third harmonic back potential.

In order to suppress the torque pulsation of PMSM used in aviation electromechanical actuation systems and enhance the reliability of the managed system, due to the complicated working surroundings of PMSM in aviation electromechanical actuation systems and frequent workload changes, the dynamic performance of the motors is required to be higher. In this paper, a fuzzy-ADRC torque ripple suppression technique of PMSM primarily based on a three-phase four-bridge inverter is proposed. In this method, a three-phase four-bridge inverter is used to change the three-phase three-bridge inverter, and the fourth bridge arm of the three-phase four-bridge inverter can filter out the contemporary harmonics when the load changes, so as to suppress the torque ripple of the motor. The ADRC is used to substitute PI control to control the motor. The ADRC makes use of the prolonged state observer (ESO) to observe the essential variables of the PMSM device to track and compensates for the control system with the observed values in the feedback control link, which solves the problem where the response speed and overfire of PI control are hard to balance. On this basis, the Kalman filter is brought to the motor speed ring to similarly enhance the ADRC and enhance the steadiness of the motor speed control. The fuzzy control can regulate the parameters of the nonlinear error feedback control rate in the ADRC in real time, enhance the balance of the system, solve the problem that there are too many ADRC parameters and the setting is too complicated, and similarly enhance the torque pulsation suppression overall performance of PMSM. Simulation consequences exhibit that the proposed technique is correct and effective.

2. Mathematical Model of PMSM

The motor studied in this paper is a surface-mounted PMSM. The stator voltage equation for the PMSM in the rotating coordinate system is

$$\begin{cases} U_{\mathrm{d}} = L_{\mathrm{d}}\frac{di_{\mathrm{d}}}{d_{\mathrm{t}}} + R_{\mathrm{s}}i_{\mathrm{d}} - \omega_{\mathrm{e}}L_{\mathrm{q}}i_{\mathrm{q}} \\ U_{\mathrm{q}} = L_{\mathrm{q}}\frac{di_{\mathrm{q}}}{d_{\mathrm{t}}} + R_{\mathrm{s}}i_{\mathrm{q}} + \omega_{\mathrm{e}}L_{\mathrm{d}}i_{\mathrm{d}} + \omega_{\mathrm{e}}\psi_{\mathrm{f}} \end{cases} \tag{1}$$

In the formula, i_{d} and i_{q} are the currents of the d-axis and q-axis, U_{d} and U_{q} are the voltages of the d-axis and q-axis, L_{d} and L_{q} are the inductances of the d-axis and q-axis, ω_{e} is the electric angular velocity; ψ_{f} is the flux link of a permanent magnet, and R_{s} is the stator phase resistance.

The $i_{\mathrm{d}} = 0$ vector control is adopted, the $i_{\mathrm{d}} = 0$ control method is used, the control method has a simple structure and small calculation amount, and the control method has no direct axis current, so there is no direct axis armature reaction, and the permanent magnet will not be demagnetized. All the currents of the motor are used to generate electromagnetic torque, and the current control rate is high. The torque equation of PMSM is

$$\begin{aligned} T_{\mathrm{e}} &= \tfrac{3}{2}p\left[\psi_{\mathrm{f}}i_{\mathrm{q}} + \left(L_{\mathrm{d}} - L_{\mathrm{q}}\right)i_{\mathrm{d}}i_{\mathrm{q}}\right] \\ &= \tfrac{3}{2}p\psi_{\mathrm{f}}i_{\mathrm{q}} = k_{\mathrm{t}}i_{\mathrm{q}} \end{aligned} \tag{2}$$

where T_{e} is the torque; k_{t} is the torque coefficient, and $k_{\mathrm{t}} = 1.5\mathrm{p}\psi_{\mathrm{f}}$; p is the number of pole pairs.

The equation of the mechanical motion of the motor is as follows:

$$J\frac{d\Omega_{\mathrm{m}}}{dt} = T_{\mathrm{e}} - T_{\mathrm{L}} - B_{\mathrm{m}}\Omega_{\mathrm{m}} \tag{3}$$

where J is the moment of inertia of the rotor; T_{L} is the load torque; B_{m} is the viscosity coefficient.

3. Mathematical Model of the Aviation Electromechanical Transmission System

The aviation electromechanical actuation system mainly includes a clutch, roller screw, and push rod. The electromechanical actuation system transfers the output torque of the PMSM to the screw of the roller screw via the clutch and converts the rotating motion of the motor into linear displacement via this process. The mechanical and electrical actuation system composed of the clutch, roller screw, and push rod is modeled equivalently. Firstly, the controlled system is analyzed by a dynamic model, which can be generally equivalent to Figure 1.

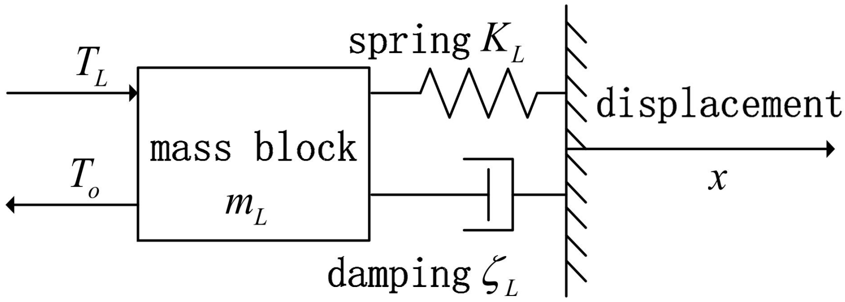

Figure 1. Load dynamics model.

In Figure 1, T_L and T_O, respectively, represent the driving force required by the load and the torque caused by the load interference; K_L is the elastic spring coefficient; ζ_L is the damping coefficient of the system; m_L is the mass of the mass block in the load; and x is the displacement. According to the load dynamics model, the following can be obtained:

$$T_{\mathrm{L}}(t) = T_{\mathrm{o}}(t) + m_{\mathrm{L}}\frac{\mathrm{d}^2x(t)}{\mathrm{d}t^2} + \xi_{\mathrm{L}}\frac{\mathrm{d}x(t)}{\mathrm{d}t} + K_{\mathrm{L}}x(t) \tag{4}$$

Applying the Laplace transform to the above equation gives

$$T_{\mathrm{L}}(s) = T_{\mathrm{o}}(s) + \left(m_{\mathrm{L}}s^2 + \xi_{\mathrm{L}}s + K_{\mathrm{L}}\right)x(s) \tag{5}$$

According to the above formula, the transmission mechanism of the aviation electromechanical actuation system is equivalent to Figure 2.

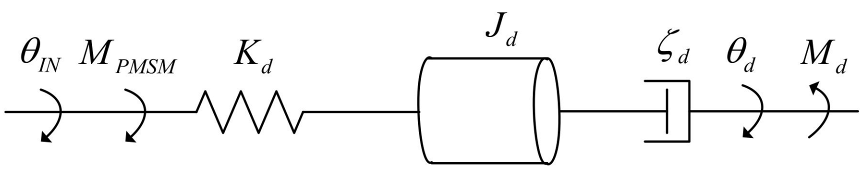

Figure 2. Equivalent model of transmission mechanism of aviation electromechanical actuation system.

Among them, θ_{IN} and M_{PMSM} are, respectively, the rotation angle of the PMSM and the torque transmitted to the mechanical transmission mechanism; K_d represents the equivalent torsional stiffness of the roller screw; J_d represents the equivalent moment of inertia; ζ_d represents the damping coefficient; θ_d represents the angular displacement of the ball screw obtained after the load-displacement distance is converted; and M_d is the resistance of the roller screw. According to the above model, the equations of motion and torque of the mechanical transmission system of the electromechanical actuation actuator can be obtained as follows:

$$\begin{cases} J_{\mathrm{d}}\frac{\mathrm{d}^2\theta_{\mathrm{d}}(t)}{\mathrm{d}^2t} + \xi_{\mathrm{d}}\frac{\mathrm{d}\theta_{\mathrm{d}}(t)}{\mathrm{d}t} + M_{\mathrm{d}}(t) = M_{\mathrm{PMSM}}(t) \\ K_{\mathrm{d}}[\theta_{\mathrm{d}}(t) - \theta_{\mathrm{IN}}(t)] = M_{\mathrm{PMSM}}(t) \end{cases} \tag{6}$$

The Laplace transform of the above equation gives

$$\begin{cases} J_{\mathrm{d}}s^2\theta_{\mathrm{d}}(s) + \xi_{\mathrm{d}}s\theta_{\mathrm{d}}(s) + M_{\mathrm{d}}(s) = M_{\mathrm{PMSM}}\ (s) \\ K_{\mathrm{d}}[\theta_{\mathrm{IN}}(s) - \theta_{\mathrm{d}}(s)] = M_{\mathrm{PMSM}}\ (s) \end{cases} \tag{7}$$

After sorting out the above formula, we obtain

$$\theta_{\mathrm{d}}(s) = \frac{K_{\mathrm{d}}\theta_{\mathrm{IN}}(s) - M_{\mathrm{d}}(s)}{J_{\mathrm{d}}s^2 + \xi_{\mathrm{d}}s + K_{\mathrm{d}}} \tag{8}$$

The rotation angle of the roller screw 1 is converted into the linear displacement of the push rod 2 to obtain

$$x = \frac{\theta_d P_h}{2\pi} \quad (9)$$

In the above formula, P_h is the lead of the roller lead screw.

4. Three-Phase Four-Leg Inverter

The three-phase four-bridge arm inverter connects the fourth bridge arm to the motor center line to solve the problem of capacitor neutral point imbalance and overmargin, and the inductor with a neutral line in the series can filter out the switching ripple when the motor load changes, acting as a filter.

When the load of a PMSM changes abruptly, the current and torque of the motor fluctuate violently under the influence of sudden load. The three-phase four-bridge inverter has the function of a filter, which can filter out the current harmonics induced by using the unexpected change of the motor load, thus reducing the torque and current ripple of the motor and avoiding the problem of motor efficiency reduction caused by current harmonics caused by complex sudden change.

The three-phase four-bridge inverter is shown in Figure 3.

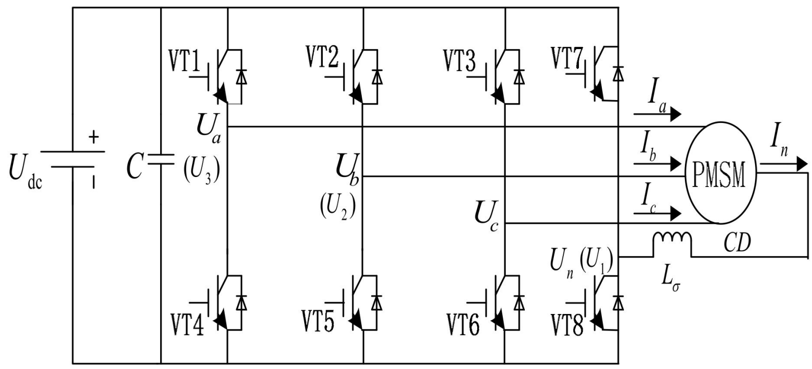

Figure 3. Topology of three-phase four-bridge inverter.

In Figure 3, VT1 and VT4 form the A bridge arm; VT2 and VT5 form the B bridge arm; VT3 and VT6 form the C bridge arm; VT7 and VT8 form the fourth bridge arm. U_{dc} is the DC voltage source; L_σ is the additional inductance. U_a, U_b, and U_c are the output voltages; I_a, I_b, and I_c are currents of the inverter; U_N and I_N represent the voltage and current of the fourth bridge arm of the inverter.

Suppose the midline current is i_N, the zero-axis current can be expressed as i_0 as follows:

$$i_N = -\sqrt{3} i_0 \quad (10)$$

It can be seen from Formula (10) that the line current i_0 can be controlled indirectly by controlling the change of the zero-axis current i_N. In normal operation, the center line current i_N is 0, which only needs to control the zero-axis current i_0, which is 0.

The PMSM normal operation is as follows:

$$i_N = -\sqrt{3} i_0 = 0 \quad (11)$$

At this time, the three-phase currents are, respectively,

$$\begin{cases} i_A = \sqrt{\frac{2}{3}}\left(i_d \cos\theta_r - i_q \sin\theta_r\right) \\ i_B = \sqrt{\frac{2}{3}}\left[i_d \cos\left(\theta_r - \frac{2}{3}\pi\right) - i_q \sin\left(\theta_r - \frac{2}{3}\pi\right)\right] \\ i_C = \sqrt{\frac{2}{3}}\left[i_d \cos\left(\theta_r + \frac{2}{3}\pi\right) - i_q \sin\left(\theta_r + \frac{2}{3}\pi\right)\right] \end{cases} \quad (12)$$

When the load changes abruptly, the three-phase output voltage can be decomposed into three balanced positive sequence, negative sequence, and zero sequence components, and the motor voltage can be expressed as

$$\begin{bmatrix} u_d \\ u_a \end{bmatrix} = U_m^p \begin{bmatrix} \cos\alpha_p \\ -\sin\alpha_p \end{bmatrix} + U_m^N \begin{bmatrix} \cos(2\omega t + \alpha_N) \\ -\sin(2\omega t + \alpha_N) \end{bmatrix} \tag{13}$$

where U_m^p and U_m^N are the voltage peaks of positive sequence and negative sequence, respectively; α_p and α_N are the initial phases of positive and negative sequence voltages, respectively.

5. Design of Active Disturbance Rejection Controller

The tracking differentiator (TD) extracts the signal of the managed object, and the extended state observer (ESO) compensates for the whole disturbance inside and outside the device to enhance the safety and balance of the system. Then, the signal extracted by the TD is used as the input of the nonlinear state error feedback control law (NLSEF). The total control value of the fuzzy-ADRC is obtained by combining the output of the NLSEF control rate with the total disturbance compensation value of the extended state observer.

The structure diagram of ADRC is shown in Figure 4.

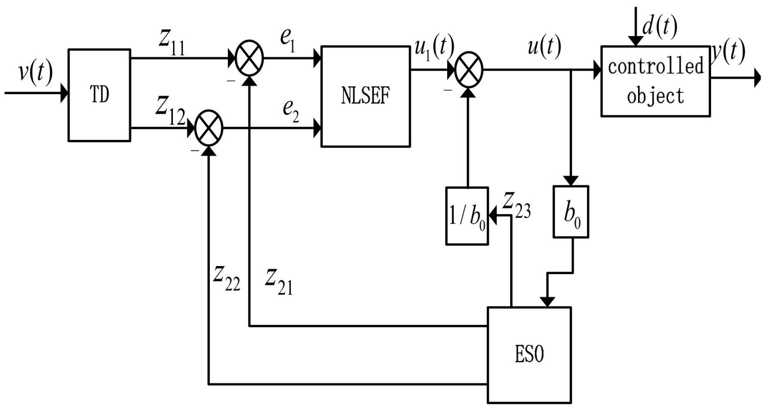

Figure 4. Structure block diagram of ADRC.

5.1. Tracking Differentiator

As the input part of the ADRC, the TD creates a reasonable arrangement for the input signal transition to solve the overshoot problem of PI control.

The standard form of a TD is as follows:

$$\left.\begin{array}{l} e_0 = z_{11} - v \\ \dot{z}_{11} = z_{12} \\ \vdots \\ \dot{z}_{1\mathrm{n}-1} = z_{1\mathrm{n}} \\ \dot{z}_{1\mathrm{n}} = -r^n \mathrm{fal}(e_0, \alpha_0, \delta_0) \end{array}\right\} \tag{14}$$

where v is the input signal, and its tracking value z_{11} can reflect the performance of TD; z_{12} to z_{1n} are the differentials of the trace values; the speed factor is r. Function fal in the formula can reduce the high-frequency oscillation of the system, and the expression of fal is as follows:

$$\mathrm{fal}(\varepsilon, \alpha, \delta) \begin{cases} |e|_\alpha sign(e), |e| > \delta \\ e/\delta^{(1-\alpha)}, \left|e\right| \le \delta \end{cases} \tag{15}$$

In the formula, α is defined as a nonlinear factor; ε is the system tracking error; δ is the filtering factor of the fal function. The larger the filtering factor, the better the filtering effect, but this will lead to tracking delay. When $\alpha = 1$, $\mathrm{fal}(e, \alpha, \delta) = e$. When $\alpha < 1$, fal has the peculiarity of "small error with large gain, large error with small gain".

5.2. Extended State Observer

ESO re-extends the output value of the controlled object into a variable and estimates and compensates for the system disturbance by each derivative signal $z_{\mathrm{i}}(t)$; the output signal $y(t)$ and the system disturbance are estimated by signal $z_{\mathrm{n}+1}(t)$, and a new state variable is obtained. The new state variable equation obtained through the above process is

$$\left.\begin{array}{l} e_1 = z_{21} - y \\ \dot{z}_{21} = z_{22} - \beta_1 \mathrm{fal}(e_1, \alpha_1, \delta_1) \\ \dot{z}_{22} = z_{23} - \beta_2 \mathrm{fal}(e_1, \alpha_1, \delta_1) \\ \vdots \\ \dot{z}_{2\mathrm{n}-1} = z_{2\mathrm{n}} - \beta_{\mathrm{n}-1} fal(e_1, \alpha_1, \delta_1) + bu \\ \dot{z}_{2\mathrm{n}} = -\beta_{\mathrm{n}} \mathrm{fal}(e_1, \alpha_1, \delta_1) \end{array}\right\} \tag{16}$$

In Formula (16), b is the estimated value of the system, $z_{2i}(i = 1, 2, \cdots, n-1)$ is the observed value of each order variable of the system, $z_{2\mathrm{n}}$ is the total disturbance, β_1 and β_2 represent the gain coefficients of the ESO, and u represents the output value of the ADRC.

5.3. Nonlinear State Error Feedback Control Law

The application of nonlinear functions in ADRC can effectively deal with the overshoot problem of the controlled system. Error signal and error differential signal of the transition process are generated based on the tracking differentiator method, and finally, the error integral signal is generated. The state error feedback control rate is obtained by combining the error, error differential, and error integral. The n-order nonlinear feedback expression is as follows:

$$\left\{\begin{array}{l} e_2 = z_{11} - z_{21} \\ \vdots \\ e_{\mathrm{n}+1} = z_{1\mathrm{n}} - z_{2\mathrm{n}} \\ u_0 = \beta_1 \mathrm{fal}(z_{11} - z_{21}, \alpha, \delta) + \cdots + \beta_{\mathrm{n}} fal(z_{1\mathrm{n}} - z_{2\mathrm{n}}, \alpha, \delta) \\ u = u_0 - \frac{z_{2\mathrm{n}+1}}{b} \end{array}\right. \tag{17}$$

where $e(i = 2, 3, \cdots, n+1)$ is the difference between the input value and each order differential value of the controlled quantity. z_{11} is the trace value of the input value v, z_{12} to z_{1n} are the differentials of the trace values, and $z_{2i}(i = 1, 2, \cdots, n-1)$ is the observed value of each order variable of the system. δ, α, and u_0 are the filter factor, the nonlinear factor, and the feedback output of the NLSEF, respectively.

5.4. Improved Active Disturbance Rejection Control

To enhance the technology of the ADRC of PMSM to effectively suppress the torque ripple, the Kalman filter is added to the loop ADRC of PMSM.

Assume that the controlled system is a discrete system and is perturbed, and its output equation and state equation are

$$\left\{\begin{array}{l} y(k) = H(k)x(k) + \rho(k) \\ x(k) = A(k|k-1)x(k-1) + B(k-1)u(k-1) + r(k-1) \end{array}\right. \tag{18}$$

In the above formula, $x(k)$ and $y(k)$ are the system state and output value; $u(k)$ represents the control quantity of the controlled at moment k; $A(k|k-1)$, B, and H, respectively, represent the transfer matrix, system matrix, and measurement matrix of the controlled system; r is the process noise of the system; ρ is the measurement noise received during the measurement process. It can be assumed that r and ρ are Gaussian white noise, and the mean value of the signal is 0; then, r and ρ meet the following conditions:

$$\begin{cases} E(r) = 0 \\ E(\rho) = 0 \\ \operatorname{cov}(r) = E\left[rr^T\right] = Q \\ \operatorname{cov}(\rho) = E\left[\rho\rho^T\right] = R \\ \operatorname{cov}(r\rho) = E\left[r\rho^T\right] = 0 \end{cases} \tag{19}$$

In Formula (19), Q and R are both covariance matrices.

Kalman filter control is mainly divided into two processes: the first process is prediction, and the second process is correction. In the prediction process, $\hat{x}(k)$ and $P(k)$ of the controlled system at moment k should be promptly corrected, and the corresponding state-predicted value and error covariance matrix at moment $k+1$ of the next time point should be obtained. The calculation formula of this process is as follows:

$$\begin{cases} \hat{x}(k+1|k) = A(k+1|k)\hat{x}(k) + B(k)u(k) \\ P(k+1|k) = A(k+1|k)P(k)A^T(k+1|k) + Q \end{cases} \tag{20}$$

In the above formula, $\hat{x}(k)$ and $P(k)$, respectively, represent the state-predicted value and error covariance matrix at time k; $\hat{x}(k+1|k)$ and $P(k+1|k)$ are the state-predicted value and error covariance matrix when the time is $k+1$.

The correction process of the Kalman filter includes three steps: calculation of the gain, correction of the state estimate obtained in the prediction process, and correction of the error covariance obtained in the process of making predictions. The above calculation process is shown in Formula (21):

$$\begin{cases} K(k+1) = P(k+1|k)H^T(k+1) * \left(H(k+1)P(k+1|k)H^T(k+1) + R\right)^{-1} \\ \hat{x}(k+1) = \hat{x}(k+1|k) + K(k+1)(y(k+1) - H(k+1)\hat{x}(k+1|k)) \\ P(k+1) = P(k+1|k) - K(k+1)H(k+1)P(k+1|k) \end{cases} \tag{21}$$

From Formula (21), $K(k+1)$ represents the gain calculation, $\hat{x}(k+1)$ represents the correction of the state predicted value from the prediction when the time is k, and $P(k+1)$ represents the correction of the error covariance from the prediction at time k.

6. Design of Fuzzy Active Disturbance Rejection Controller

Although compared with PID control, ADRC can improve the torque ripple suppression ability of the motor to some extent, more parameters need to be adjusted for ADRC, which increases the difficulty of parameter adjustment in the actual control process. However, according to the real-time state change of the controlled system, fuzzy control adjusts the parameters of ADRC. The first step of fuzzy control is fuzzization, the second step is fuzzy reasoning, and the third step is defuzzification. Fuzzy control solves the complex problem of parameter tuning of ADRC.

Fuzzy control first converts the input quantity into fuzzy quantity via fuzzification; then, the fuzzy quantity collected in the previous step is applied to the fuzzy inference process via the fuzzy rules; and finally, the fuzzy quantity obtained by fuzzy inference is converted into the precise quantity required by control by fuzzification. A second-order ADRC is used here. The principle of fuzzy-ADRC is shown in Figure 5.

In the above figure, e_1 and e_2 are the input quantity of fuzzy control, $\Delta\beta_0$; $\Delta\beta_1$ and $\Delta\beta_2$ are the exact output after unfuzzing; and the fuzzy subset is set as {"negative large (NB)", "negative medium (NM)", "negative small (NS)", "zero (ZO)", "positive small (PS)", "middle (PM)", "positive large (PB)"}.

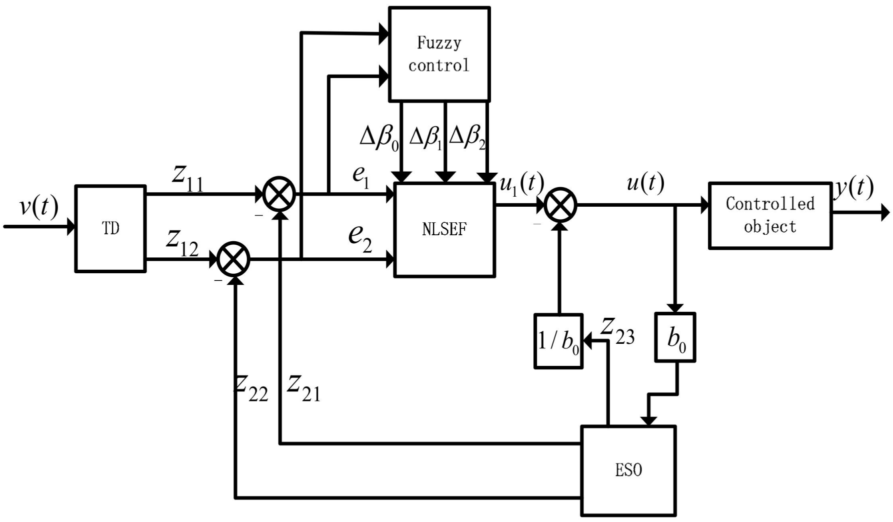

Figure 5. Structure diagram of fuzzy-ADRC.

Here, the membership functions of $\Delta\beta_0$, $\Delta\beta_1$, and $\Delta\beta_2$ are set to a triangular shape, and the rule functions of the input and output of fuzzy control are set to the membership function form of the middle triangle of the normal distribution on both sides. The basic discourse domain of e_1 and e_2 is set as $[-3, 3]$. The fundamental domain of $\Delta\beta_0$ and $\Delta\beta_1$ is $[-0.3, 0.3]$, and the fundamental domain of $\Delta\beta_2$ is $[-0.06, 0.06]$. The Mandani method is used for fuzzy reasoning of fuzzy control, and the center of gravity method is used in the process of defuzzification. Figure 6 shows the regular function curves of e_1 and e_2, Figure 7 shows the regular function curves of $\Delta\beta_0$ and $\Delta\beta_1$, and Figure 8 shows the regular function curves of $\Delta\beta_2$.

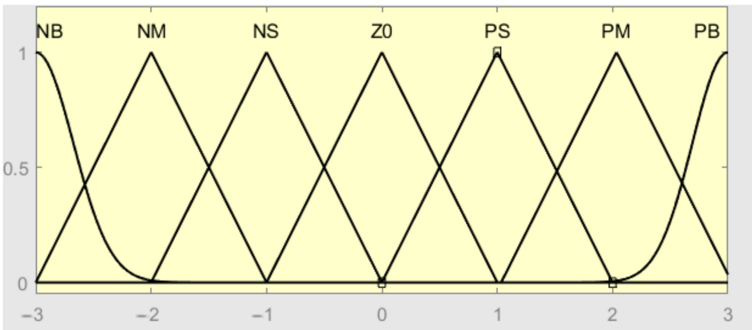

Figure 6. Regular function curves of e_1 and e_2.

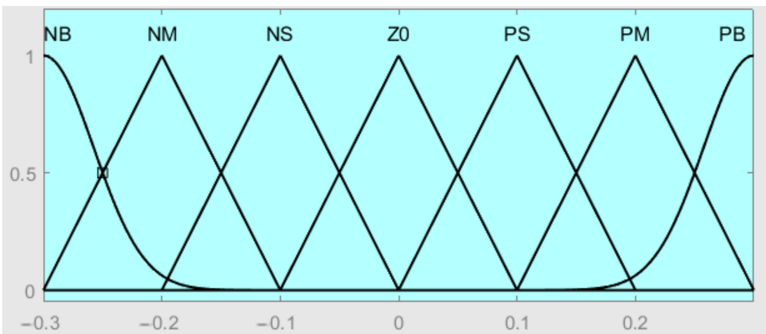

Figure 7. Regular function curves of $\Delta\beta_0$ and $\Delta\beta_1$.

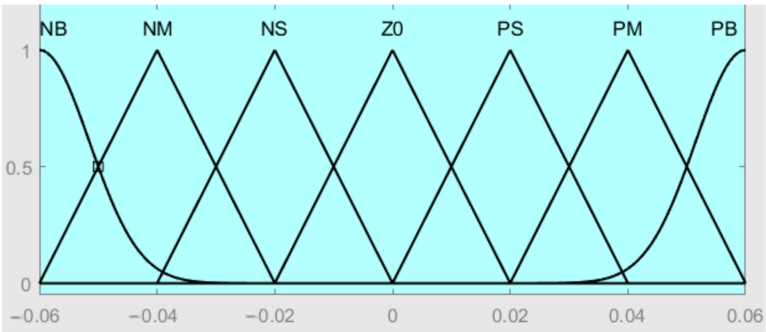

Figure 8. Regular function curves of $\Delta\beta_2$.

The fuzzy control rules with correction coefficients $\Delta\beta_0$, $\Delta\beta_1$ and $\Delta\beta_2$ are shown in Tables 1–3.

Table 1. $\Delta\beta_0$ Fuzzy rules table.

e_1 \ e_2	NB	NM	NS	ZO	PS	PM	PB
NB	NB	NB	NM	NM	NS	ZO	ZO
NM	NB	NB	NM	NS	NS	ZO	ZO
NS	NB	NM	NS	NS	ZO	PS	PS
ZO	NM	NM	NS	ZO	PS	PM	PM
PS	NM	NS	ZO	PS	PS	PM	PB
PM	ZO	ZO	PS	PS	PM	PB	PB
PB	ZO	ZO	PS	PM	PM	PB	PB

Table 2. $\Delta\beta_1$ Fuzzy rules table.

e_1 \ e_2	NB	NM	NS	ZO	PS	PM	PB
NB	PB	PB	PM	PM	PS	ZO	ZO
NM	PB	PB	PM	PS	PS	ZO	NS
NS	PM	PM	PM	PS	ZO	NS	NS
ZO	PM	PM	PS	ZO	NS	NM	NM
PS	PS	PS	ZO	NS	NS	NM	NM
PM	PS	ZO	NS	NM	NM	NM	NB
PB	ZO	ZO	NM	NM	NM	NB	NB

Table 3. $\Delta\beta_2$ Fuzzy rules table.

e_1 \ e_2	NB	NM	NS	ZO	PS	PM	PB
NB	PS	NS	NB	NB	NB	NM	PS
NM	PS	NS	NB	NM	NM	NS	ZO
NS	ZO	NS	NM	NM	NS	NS	ZO
ZO	ZO	NS	NS	NS	NS	NS	ZO
PS	ZO	ZO	ZO	ZO	ZO	ZO	ZO
PM	PB	PS	PS	PS	PS	PS	PB
PB	PB	PM	PM	PM	PS	PS	PB

The surface diagrams of $\Delta\beta_0$, $\Delta\beta_1$, and $\Delta\beta_2$ obtained according to fuzzy rules are shown in Figure 9.

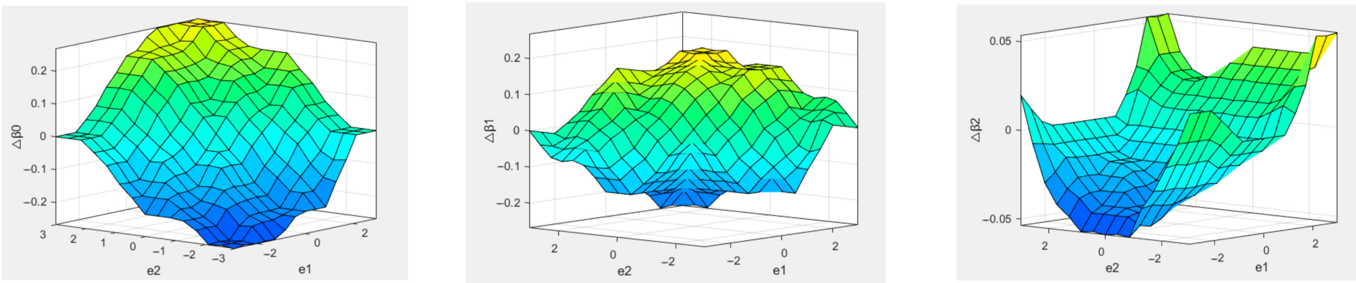

(**a**) (**b**) (**c**)

Figure 9. Fuzzy regular surface diagram. (**a**) Input and output surface diagram of $\Delta\beta_0$; (**b**) input and output surface diagram of $\Delta\beta_1$; (**c**) input and output surface diagram of $\Delta\beta_2$.

By using the weighted average method (gravity center method) to deblur e_1 and e_2 of the fuzzy-ADRC, the value of the correction coefficient can be obtained. By adding the correction parameters of the NLSEF control rate to the initial gain parameters β_0, β_1 and β_2, the calculation formula of the total gain of the system can be obtained as follows:

$$\begin{cases} \beta_0 = \beta_0' + \Delta\beta_0 \\ \beta_1 = \beta_1' + \Delta\beta_1 \\ \beta_2 = \beta_2' + \Delta\beta_2 \end{cases} \tag{22}$$

7. Stability Analysis of Control System

Assume that the controlled system is

$$\ddot{y} = -a\dot{y} - by + w_e + bu \tag{23}$$

In Formula (23), u is the system input, y is the system output, w_e is the external interference of the system, and b is the estimated value of the system, which is set as the constant b_0 in this system. By sorting out the above formula, we obtain

$$\ddot{y} = -a\dot{y} - by + w_e + (b - b_0)u = f(x_1, x_2, w(t), t + b_0 u) \tag{24}$$

Organize the above formula into the form of an equation of state:

$$\begin{cases} \dot{x}_1 = x_2 \\ \dot{x}_2 = f(x_1, x_2, w(t), t) + b_0 u \\ y = x_1 \end{cases} \tag{25}$$

where $f(x_1, x_2, w(t), t)$ is the total disturbance. Expand $f(x_1, x_2, w(t), t)$ to the new state variable x_3, which is $x_3 = f(x_1, x_2, w(t), t)$, and set $\dot{x}_3 = F(t)$; then, Formula (25) becomes

$$\begin{cases} \dot{x}_1 = x_2 \\ \dot{x}_2 = x_3 + b_0 u \\ \dot{x}_3 = F(t) \\ y = x_1 \end{cases} \tag{26}$$

By sorting out the above formula, we obtain

$$\begin{cases} \dot{x} = Ax + Bu + EF(t) \\ y = Cx \end{cases} \tag{27}$$

In Formula (27), $A = \begin{bmatrix} 0 & 1 & 0 \\ 0 & 0 & 1 \\ 0 & 0 & 0 \end{bmatrix}$, $B = \begin{bmatrix} 0 \\ b_0 \\ 0 \end{bmatrix}$, $C = \begin{bmatrix} 1 & 0 & 0 \end{bmatrix}$, $E = \begin{bmatrix} 0 \\ 0 \\ 1 \end{bmatrix}$.

The concrete form of the extended state observer in this design can be rewritten as

$$\begin{cases} \dot{x} = AZ + Bu + EF(t) + L(y - \hat{y}) \\ \hat{y} = CZ \end{cases} \tag{28}$$

In Formula (28), Z is the new system state after expansion, $\hat{y}$ is the estimated possible output, and $L = \begin{bmatrix} \beta_1 & \beta_2 & \beta_3 \end{bmatrix}$ is the gain matrix.

To facilitate the analysis of its stability, the general form of the extended state observer is written as

$$\begin{cases} \dot{z} = Az + B[f(x,t) + b_0 u] + K(y - \hat{y}) \\ \hat{y} = Cz \end{cases} \tag{29}$$

The output tracking error of $e = y - \hat{y}$, z is an estimate of x, defined as $\widetilde{e} = e - \hat{e}$, $\hat{e} = \hat{y} - x = \left[\hat{e}, \dot{\hat{e}}, \ddot{\hat{e}}\right]^T$, $e = z - x = \left[e, \dot{e}, \ddot{e}\right]^T$, and the control target is $\lim_{t\to\infty} \| e(t) \| = 0$.

And because K is a gain matrix of $[1 \times 3]$, assuming that $K = [k_1, k_2, k_3]$, (A, B) is controllable, a reasonable choice of k_i makes it a Hurwitz-characteristic polynomial.

The ideal control law is as follows:

$$u* = \frac{1}{b_0}\left[-f(x,t) + \dddot{y} + K^T e\right] \tag{30}$$

By combining Formulas (29) and (30), we obtain:

$$\dddot{e} + k_3 \ddot{e} + k_2 \dot{e} + k_1 = 0 \tag{31}$$

The ideal $u*$ cannot be obtained, so the supervisory variable u_0 is introduced here.

$$u* = u_0 + u_c \tag{32}$$

In the above formula, u_c is the compensation of fuzzy control approximation and interference error.

The output of the fuzzy system is

$$\hat{f}(x) = \frac{\sum\limits_{i=1}^{\mathrm{r}} f^i \left(\prod\limits_{j=1}^{\mathrm{n}} \mu_{A_j^i}(x_j) \right)}{\sum\limits_{i=1}^{\mathrm{r}} \left(\prod\limits_{j=1}^{\mathrm{n}} \mu_{A_j^i}(x_j) \right)} = \theta^{\mathrm{T}} \xi(x) \tag{33}$$

In Formula (33), r is the number of fuzzy rules, which is 49 in this paper; $\mu_{A_j^i}(x_j)$ is the membership function of fuzzy set A_j^i; and $\theta = [\theta_1, \cdots, \theta_r]^T$ is the afterpart of fuzzy rules, which is determined according to the partial membership function center of each afterpart of fuzzy rules. $\xi = \left[\xi^1, \xi^2, \cdots, \xi^r\right]^T$ is the fuzzy basis function.

$$\xi^i(x) = \frac{\left(\prod\limits_{j=1}^{n} \mu_{A_j^i}(x_j) \right)}{\sum\limits_{i=1}^{r} \left(\prod\limits_{j=1}^{n} \mu_{A_j^i}(x_j) \right)} \tag{34}$$

Let us say there is at least one $\sum\limits_{i=1}^{r} \left(\prod\limits_{j=1}^{n} \mu_{A_j^i}(x_j) \right) > 0$.

Simultaneously, Formulas (30) and (33) give

$$u_0 = \frac{1}{b_0}\left[-\hat{f}(\theta) + \dddot{y} + K^T e\right] \tag{35}$$

Define θ_f^* as the ideal parameter variable for control rate $u*$:

$$\theta_f^* = \underset{\theta \in \Omega_\theta}{\operatorname{argmin}} \left[\sup_{x \in \Omega_\theta} \left| \hat{f}(x) - f(x) \right| \right] \quad (36)$$

In Formula (36), Ω_θ represents the boundary set of θ, and the ideal parameter vector θ_f^* is a constant introduced for the convenience of analysis, and its specific value does not need to be defined in the realization of control.

Suppose $\left\| \theta_f^* \right\|$ is bounded, that is $\left\| \theta_f^* \right\| \leq M_\theta$, and M_θ is an unknown normal number; then, the optimal disturbance function of the fuzzy system becomes $\hat{f}(\theta_f^*)$.

Then, the tracking error of the system can be expressed as

$$\dot{e} = \left[A - BK^T \right] e + B \left[\hat{f}(\theta_f^*) - f(\theta_f) \right] \quad (37)$$

The minimum approximation error of fuzzy-ADRC is as follows:

$$\varepsilon(x) = \left[\hat{f}(\theta_f^*) - f(\theta_f) \right] \quad (38)$$

Then, Formula (37) can be expressed as

$$\dot{e} = \left[A - BK^T \right] x + B \left[\hat{f}(\theta_f) - \hat{f}(\theta_f^*) + \varepsilon(x) \right] \quad (39)$$

Substitute the above formula into Formula (33) to obtain

$$\dot{e} = \left[A - BK^T \right] x + B \left[(\theta_f^* - \theta_f)^T \xi(x) + \varepsilon(x) \right] \quad (40)$$

Let $\widetilde{\theta} = \theta_f - \theta_f^*$; we can obtain

$$\dot{e} = \left[A - BK^T \right] e + B \left[-\widetilde{\theta}_f^T \xi(x) + \varepsilon(x) \right] \quad (41)$$

Define $A_c = \left[A - BK^T \right] = \begin{pmatrix} 0 & 1 & 0 \\ 0 & 0 & 1 \\ -k_1 & -k_2 & -k_3 \end{pmatrix}$, and $b_c = \begin{pmatrix} 0 \\ 0 \\ 1 \end{pmatrix}$.

In order to make the system stable, that is $\lim_{t \to \infty} \| e(t) \| = 0$, it is necessary to select appropriate parameters such that the roots of the polynomial $s_3 + k_3 s^2 + k_2 s + k_1 = 0$ are in the left half-plane of the coordinate system; then, A_c is a stable matrix, and there is a positive definite matrix P that satisfies

$$A_c^T P + P A_c = -Q \quad (42)$$

According to Lyapunov's second method, a positive definite function V is assumed. In order to verify the stability of the system, considering the tracking error and the parameter error in the position function, the positive definite function is defined as follows:

$$V = \frac{1}{2} e^T P e + \frac{1}{2r} \widetilde{\theta}_f^T \widetilde{\theta}_f \quad (43)$$

Take the derivative of the above formula with respect to time t:

$$\dot{V} = -\frac{1}{2} e^T Q e + e^T P B \left[-\widetilde{\theta}_f^T \zeta(x) + \varepsilon(x) \right] + \frac{1}{r} \widetilde{\theta}_f^T \dot{\widetilde{\theta}}_f \quad (44)$$

where r is a non-zero constant, design $\dot{\tilde{\theta}}_f = re^T PB\zeta(x)$; then,

$$\dot{V} = -\frac{1}{2}e^T Qe + e^T PB\varepsilon(x) \tag{45}$$

By analyzing the above Formula (45), it can be seen that $-\frac{1}{2}e^T Qe < 0$, and $\varepsilon(x)$ is the minimum approximation error of fuzzy-ADRC. According to Formula (33) and Formula (38), it can be seen that the larger the number of r is, the smaller the number of $\varepsilon(x)$ is; that is, when the number of fuzzy rules is sufficient, it can always make $\dot{V} = -\frac{1}{2}e^T Pe + e^T PB\varepsilon < 0$. According to Lyapunov's second method, the system is globally stable.

8. Design of Fuzzy Active Disturbance Rejection Control System for PMSM

Because the aviation electromechanical actuator system has high requirements for reliability and dynamics, the inverter uses a three-phase four-arm inverter with filtering performance, and the torque ripple when the motor load changes is reduced by the common mode suppression performance of the three-phase four-bridge. The speed ring of the motor is controlled by fuzzy-ADRC, and a Kalman filter is added to the speed loop to filter out current harmonics. In the design experiment, the DSP library of the ST company for complex digital signal operation processing is used to speed up the filter, and the floating-point operation unit, FPU, is opened to shorten the iterative operation time of the filter. The matrix operation function provided by the matrix operation library in the DSP library can improve the speed of filter matrix iteration operation and cause the iteration period of the Kalman filter to meet the timeliness requirement of the torque loop control. The design uses the Kalman filter to filter the speed ring, which weakens the influence of system disturbance on the speed; the parameters of the extended state observer are adjusted in real time by fuzzy control, which can improve the control speed and reduce the influence of disturbance on motor operation. The control mode of the position loop and current loop is PI control, and the $i_{\mathrm{d}}^* = 0$ control mode is adopted. Given the rotor position θ^* and the measured motor rotor position θ as the input value of the position ring, the motor input speed n^* is obtained via PI control, the measured motor speed n is obtained as the input value of fuzzy-ADRC, and the current input value i_q^* is obtained via fuzzy-ADRC. Combined with $i_{\mathrm{d}}^* = 0$, control 3D-SVPWM modulated wave generation via coordinate transformation to control the inverter and then control the operation of PMSM. Figure 10 is the principle diagram of the fuzzy-ADRC of PMSM designed in this paper.

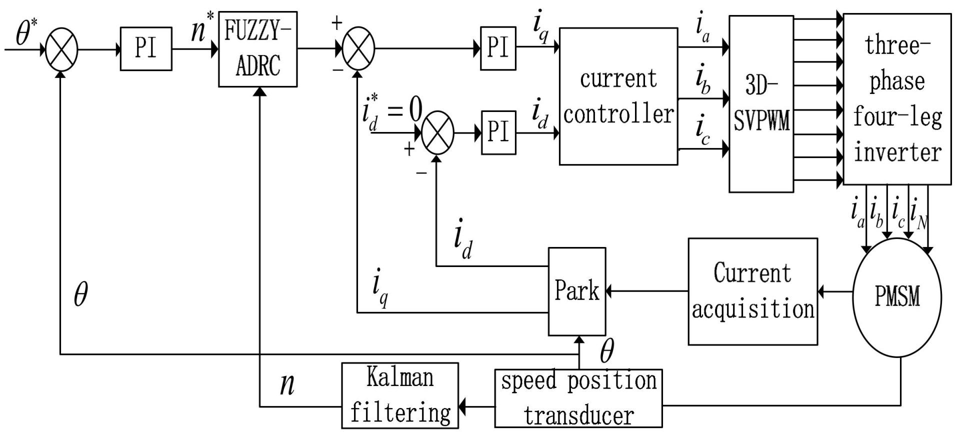

Figure 10. Fuzzy-ADRC of three-phase four-bridge inverter.

PI control parameters are P: 20 and I: 1.

The ADRC parameters are TD: r = 100, h = 0.001, alpha0 = 0.4; ESO: beta0 = 700, beta1 = 4000, beta2 = 7000, delta = 0.01, b = 0.9; NLSEF: alpha = 0.7, delta = 0.01, and k = 80.

The Kalman filter parameters are as follows:

$$Q = \begin{bmatrix} 0.1 & 0 & 0 \\ 0 & 0.1 & 0 \\ 0 & 0 & 50 \end{bmatrix}, \; R = \begin{bmatrix} 0.2 & 0 \\ 0 & 0.2 \end{bmatrix}, \; P_0 = \begin{bmatrix} 0.1 & 0 & 0 \\ 0 & 0.1 & 0 \\ 0 & 0 & 100 \end{bmatrix}$$

9. Simulation and Result Analysis

To verify the results of the fuzzy-ADRC designed in this paper on the torque ripple suppression of PMSM, Simulink was used to simulate and analyze the designed fuzzy-ADRC of PMSM. Table 4 shows the simulation parameters of PMSM used in this design.

Table 4. Parameters of PMSM.

Parameter	Value	Symbol
Stator resistance	2.8758	R_s/Ω
q-axis inductance	8.5	L_s/mH
d-axis inductance	8.5	L_s/mH
Flux linkage	2000	Ψ_m/mWb
Number of pole-pairs	4	
Rated speed	1000	ω_N/(r/min)
Moment of inertia	1×10^{-3}	J/(kg/m^2)

Figures 11 and 12, respectively, show the comparison of torque, speed, and harmonics of different inverters under PI control. The rated speed of PMSM is set to 1000 r/min, and the load torque when the motor is started is 5 N·m. At 0.5 s, the motor load suddenly increases to 10 N·m; at 1 s, the motor load suddenly decreases to 5 N·m.

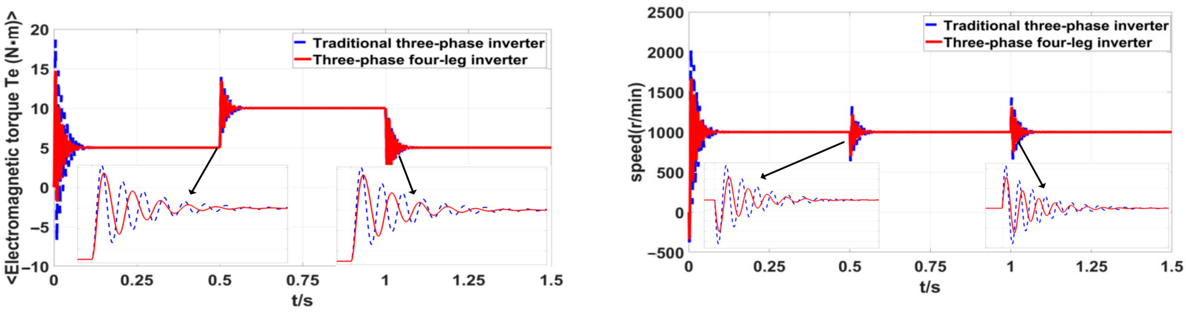

(**a**) (**b**)

Figure 11. Inverter torque speed comparison diagram. (**a**) Comparison of inverter torque; (**b**) comparison of inverter speed.

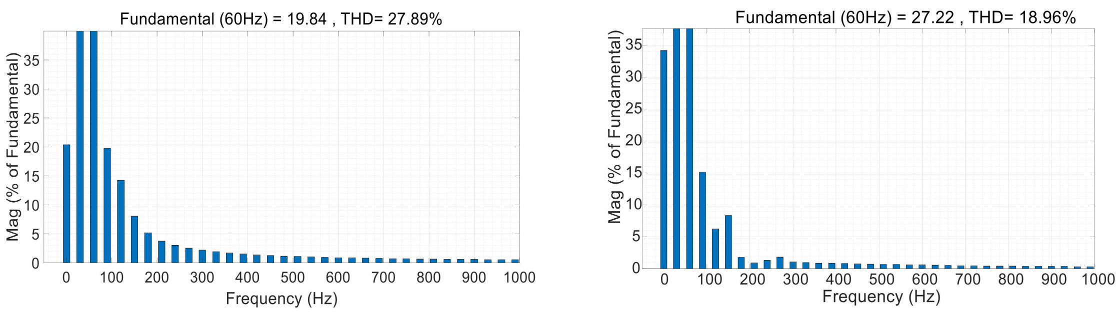

(**a**) (**b**)

Figure 12. Inverter harmonic comparison diagram. (**a**) Traditional three-phase inverter current harmonic diagram; (**b**) three-phase four-bridge inverter current harmonic diagram.

Figure 11 shows that the torque ripple and speed ripple of the PMSM controlled by the three-phase four-bridge inverter are lower than those of the motor controlled by the three-phase inverter. Figure 12 shows that the current harmonic distortion rate of the three-phase four-bridge control PMSM is 27.89%, which is lower than the total A-phase harmonic distortion rate of the traditional three-phase inverter of 18.96%.

The simulation of PMSM under ADRC, improved ADRC, and fuzzy-ADRC is carried out. The given speed is 1000 r/min, and the load torque when the motor starts is 5 N·m. At 0.05 s, the motor load suddenly increases to 10 N·m, and at 0.1 s, the motor load suddenly decreases to 5 N·m. Figures 13–15 are the simulation results.

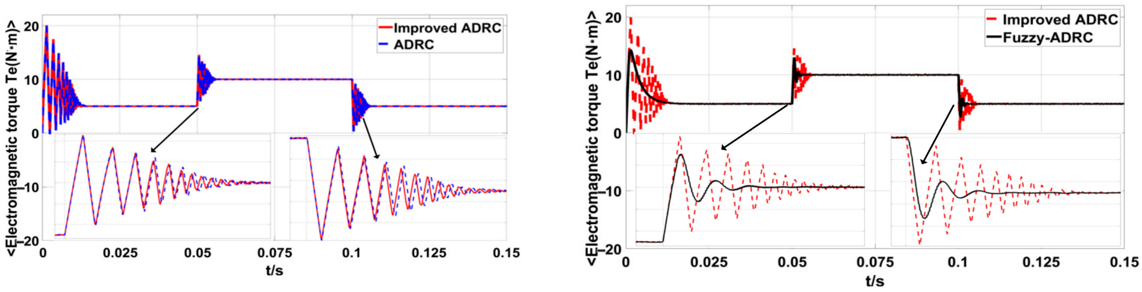

(**a**) (**b**)

Figure 13. Motor torque comparison diagram. (**a**) ADRC and improved ADRC torque diagram; (**b**) improved ADRC and fuzzy-ADRC torque diagram.

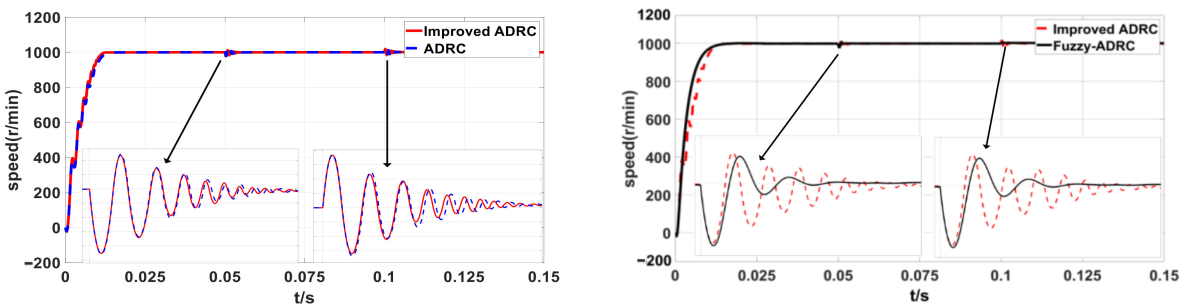

(**a**) (**b**)

Figure 14. Motor speed comparison diagram. (**a**) ADRC and improved ADRC speed diagram; (**b**) improved ADRC and fuzzy-ADRC speed diagram.

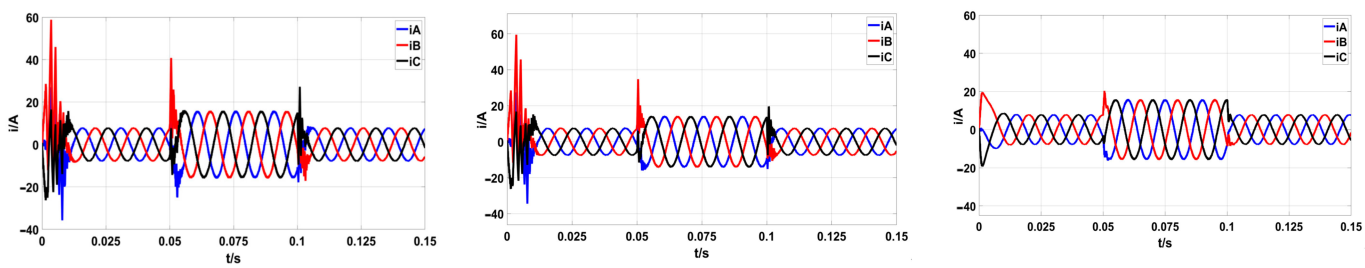

(**a**) (**b**) (**c**)

Figure 15. Motor current comparison diagram. (**a**) Motor current diagram under ADRC; (**b**) motor current diagram under improved ADRC; (**c**) motor current diagram under fuzzy-ADRC.

From Figure 13, we can see that the PMSM's starting torque under fuzzy-ADRC and the torque under sudden load change are lower than those under improved ADRC, and the motor torque pulsation under improved ADRC is lower than that under active disturbance rejection control. By comparing Figure 14, it can be seen that the speed pulsation of the PMSM under fuzzy-ADRC is lower than that under improved ADRC, while the speed pulsation under improved ADRC is lower than that under ADRC. From Figure 15, we can see that the PMSM under fuzzy-ADRC has the lowest current pulsation and the shortest recovery time.

In order to make the PMSM stop at the specified position quickly and stably, the initial position of the motor was set to 30 rad in the system for the three closed-loop control modes, and the load of PMSM changed from 5 N·m to 10 N·m after 1 s. The rotor position of PMSM under ADRC, improved ADRC, and fuzzy-ADRC were simulated, and the simulation comparison diagram is shown in Figures 16 and 17.

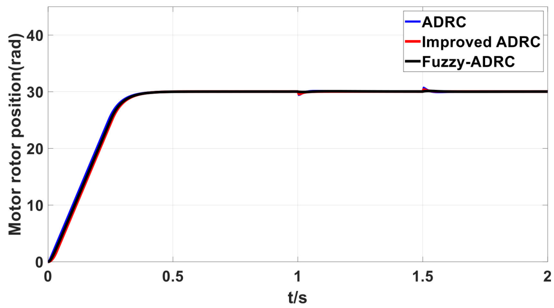

Figure 16. Motor rotor position simulation diagram.

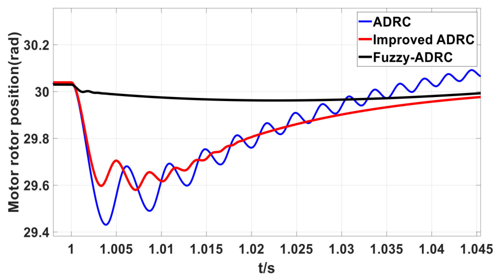

(**a**)

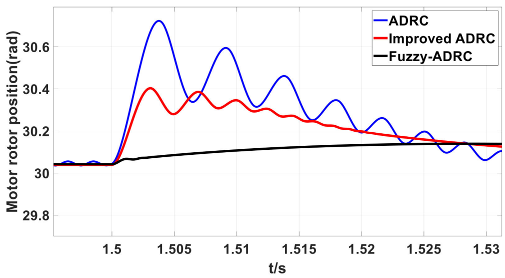

(**b**)

Figure 17. Local simulation diagram of motor rotor position. (**a**) Simulation diagram of rotor position during motor startup; (**b**) simulation diagram of rotor position of motor with sudden load reduction.

Via a comparative analysis of Figures 16 and 17, it can be seen that when the given rotor position is 30 rad, under ADRC, improved ADRC, and fuzzy-ADRC, the rotor position fluctuation of the motor under ADRC is largest when the motor load changes abruptly. The position fluctuation of the motor rotor under the improved ADRC is less than that under ADRC, and the time to return to the predetermined position is shorter. The position of the motor rotor under fuzzy-ADRC comprises basically no pulsation, and its stability is the best.

Via the above simulation experiments and analysis, it can be seen that the three-phase four-bridge PMSM can effectively suppress the torque, speed, and current ripple of the motor under fuzzy-ADRC. This control method can maintain safe and stable operation of the motor regardless of whether the motor starts with load or the load changes during operation. This greatly improves the safety and stability of the motor operation and meets the requirements of the aviation electromechanical actuator for the motor.

10. Conclusions

Via a comparative analysis of a three-phase four-arm inverter, ADRC, and fuzzy control, this paper proposes replacing the traditional inverter with a three-phase four-arm inverter, and the fuzzy-ADRC is used to control the speed of the outer loop of the

PMSM operated by the aircraft's electromechanical system. Via simulation verification, the following conclusions are drawn:

(1) The three-phase four-bridge inverter can effectively filter out current harmonics, greatly improving the stability and anti-disturbance ability of PMSM in aviation electromechanical actuator systems.
(2) The improved ADRC designed in this paper improves the disturbance rejection performance and stability of PMSM to a certain extent compared with the active disturbance rejection control.
(3) The fuzzy-ADRC designed in this paper can greatly reduce the torque, speed, and current ripple of PMSM, cause the motor to recover stable operation faster when the load changes, and improve the reliability of PMSM. It has a certain reference value for the follow-up research and engineering application of PMSM in aviation electromechanical actuation systems.

Author Contributions: Conceptualization, C.L. and H.D.; methodology, C.L.; software, C.L.; validation, C.L., H.D. and S.W.; formal analysis, C.L.; investigation, C.L.; resources, C.L.; data curation, C.L.; writing—original draft preparation, C.L.; writing—review and editing, C.L., H.D. and R.Z.; supervision, B.W. and J.C.; project administration, B.W. and J.C.; funding acquisition, B.W., J.C. and H.D. All authors have read and agreed to the published version of the manuscript.

Funding: This study was supported by the Major Science and Technology Project of Gansu Province, China (21ZD4GA005). Sponsor: Haiying Dong.

Data Availability Statement: The original contributions presented in the study are included in the article; further inquiries can be directed to the corresponding author.

Acknowledgments: The completion of this study is due to the collaborative efforts of several co-authors.

Conflicts of Interest: Author Bo Wang and Jingbo Chen were employed by the company Academy, Lanzhou Wanli Airlines Electromechanical Limited Liability Company. The remaining authors declare that the research was conducted in the absence of any commercial or financial relationships that could be construed as a potential conflict of interest.

References

1. Raj, J.A.P.S.; Asirvatham, L.G.; Angeline, A.A.; Manova, S.; Rakshith, B.L.; Bose, J.R.; Mahian, O.; Wongwises, S. Thermal management strategies and power ratings of electric vehicle motors. *Renew. Sustain. Energy Rev.* **2024**, *189*, 113874.
2. Zhang, J.; Wang, Y.; Liu, G.; Tian, G. A review of control strategies for flywheel energy storage system and a case study with matrix converter. *Energy Rep.* **2022**, *8*, 3948–3963. [CrossRef]
3. Wang, Z.; Zhou, J.; Giorgio, R. A review of architectures and control strategies of dual-motor coupling powertrain systems for battery electric vehicles. *Renew. Sustain. Energy Rev.* **2022**, *162*, 112455. [CrossRef]
4. Fu, X.; Jiang, Z.; Lv, H. Review on the development of brushless excitation and Torque Density Improvement Technology for Electrically excited synchronous Motor. *Trans. China Electrotech. Soc.* **2022**, *37*, 1689–1702.
5. Wang, Y.; Zhang, C.; Hao, W. Review on fault tolerance technology of permanent magnet motor and its drive system. *Proc. CSEE* **2023**, *42*, 351–372.
6. Gao, F.; Xu, H.; Shi, Z.; Gao, Z.; Qiang, Y. A permanent magnet synchronous motor model with improved steady-state performance predicts flux control. *J. Harbin Inst. Technol.* **2023**, *2*, 1–10.
7. Wang, X.; Cao, B.; Mao, Z.; Brandon, G.; Edwin, E. Polyphase Permanent Magnet Synchronous Motors Direct Current Model Predictive Control with Long Prediction Horizons. *IFAC-Pap.* **2023**, *56*, 2719–2726. [CrossRef]
8. MohammadHadi, K.; Mehdi, A.R.; Hasan, Z. Continuous Control Set Model Predictive Control for the optimal current control of Permanent Magnet Synchronous Motors. *Control. Eng. Pract.* **2023**, *138*, 105590.
9. Chen, Y.; Tao, D.; Wang, L. Generation Mechanism and Control of Torque Ripple in Double parallel rotor permanent magnet synchronous Motor. *Trans. China Electrotech. Soc.* **2023**, *15*, 1–14. [CrossRef]
10. Zhou, D.; Lu, L.; Yang, C. Joint simulation optimization of high speed permanent magnet motor based on genetic algorithm. *Compos. Mach. Tool Autom. Process. Technol.* **2023**, *11*, 69–73.
11. Ding, J.; Chen, T.; Fang, J. Application of harmonic injection in electromagnetic vibration suppression of electric vehicle powertrain. *J. Vib. Eng.* **2022**, *35*, 1453–1460.
12. Yu, S.; Xue, J.; Xia, P. The motion characteristics of permanent magnet synchronous motor are improved by harmonic injection method. *Mach. Des. Manuf.* **2021**, *11*, 79–82.

13. Wang, S.; Xu, J. Neural network harmonic injection torque ripple suppression method for permanent magnet synchronous motor. *Digit. Ocean. Underw. Attack Def.* **2023**, *6*, 81–88.
14. Zheng, B.; Zou, J.; Xu, Y.; Lang, X.; Yu, G. Torque Ripple Suppression Based on Optimal Harmonic Current Injection in Dual Three-Phase PMSMs Under Magnetic Saturation. *IEEE Trans. Ind. Electron.* **2022**, *69*, 5398–5408. [CrossRef]
15. Wu, Z.; Liang, Q.; Zhang, S.; Liang, J.; Yang, X. Amplitude-Phase Based Optimal Voltage Harmonic Injection for Speed Harmonic Minimization in SPMSM. *IEEE Trans. Power Electron.* **2023**, *38*, 7494–7503. [CrossRef]
16. Guo, H.; Cao, R.; Lin, X. Torque ripple suppression of non-ideal flux linkage permanent magnet synchronous motor. *J. Electr. Mach. Control.* **2022**, *26*, 63–71.
17. Hyung-Jin, Y.; Antonio, F.C.; Petros, V. Adaptive Control to Suppress Torque Ripple in Electric Vehicles. *IFAC-Pap.* **2023**, *56*, 223–228.
18. Zhang, Z.; Chen, Y.; Xie, S.; Feng, X.; Qin, H.; Zhao, C. Current harmonic suppression for Permanent-Magnet Synchronous Motor based on Notch Filter and LADRC. *Energy Rep.* **2023**, *8*, 175–182. [CrossRef]
19. Zhou, M.; Wang, Z.; Dong, S. Suppression strategy of output torque pulsation of permanent magnet motor caused by secondary DC voltage pulsation of traction inverter. *Proc. CSEE* **2023**, *43*, 8468–8478.
20. Huang, M.; Deng, Y.; Li, H.; Wang, J. Torque Ripple Suppression of PMSM Using Fractional-Order Vector Resonant and Robust Internal Model Control. *IEEE Trans. Transp. Electrif.* **2021**, *7*, 1437–1453. [CrossRef]
21. Yuan, T.; Li, T.; Zhang, Y. Research on current dual closed-loop scheme for PMSM control system utilizing cascaded PI-RC controller. *Energy Rep.* **2023**, *9*, 470–477. [CrossRef]
22. Wang, W.; Liu, C.; Liu, S.; Song, Z.; Zhao, H.; Dai, B. Current Harmonic Suppression for Permanent-Magnet Synchronous Motor Based on Chebyshev Filter and PI Controller. *IEEE Trans. Magn.* **2020**, *57*, 1–6. [CrossRef]
23. Tian, M.; Wang, B.; Yu, Y.; Dong, Q.; Xu, D. Adaptive Active Disturbance Rejection Control for Uncertain Current Ripples Suppression of PMSM Drives. *IEEE Trans. Ind. Electron.* **2023**, *71*, 2320–2331. [CrossRef]
24. Liu, C.; Hu, J.; Shang, J. Torque ripple suppression strategy of common-DC busbar open winding permanent magnet synchronous motor based on improved auto-disturbance rejection control. *Proc. CSEE* **2023**, *43*, 779–789.